Nanoscale

PAPER

View Article Online
View Journal | View Issue

Cite this: *Nanoscale*, 2014, **6**, 9110

A gravure printed antenna on shape-stable transparent nanopaper†

Hongli Zhu,[a] Binu Baby Narakathu,[b] Zhiqiang Fang,[a] Ahmed Tausif Aijazi,[c] Margaret Joyce,[c] Massood Atashbar[b] and Liangbing Hu*[a]

Received 15th April 2014
Accepted 30th May 2014

DOI: 10.1039/c4nr02036g

www.rsc.org/nanoscale

This work presents a solution-processed gravure printed antenna on robust transparent nanopaper for potential Radio Frequency Identification (RFID) application. The nanopaper, having excellent dimensional stability in water, was obtained by glutaraldehyde treatment with hydrochloric (HCl) acid as a catalyst. For the first time, a device consisting of RF components for RFIDs was printed on stable nanopaper *via* a well-developed scalable method: gravure printing. Insertion losses of −37.9 dB and −38.85 dB for the 100 lpi and 120 lpi antennas respectively were demonstrated at the maximum gain of 683.75 MHz. The RF-based responses from the printed antenna demonstrated the feasibility of using printing technology, such as gravure printing, to fabricate flexible RFID antennas for various electronic device applications. This study paves the way for the development of low cost, disposable devices comprised of biodegradable and earth abundant materials to promote greener electronics.

Introduction

Conventionally, fabricating electronics involves high-vacuum and high-temperature deposition processes, including thermal evaporation deposition, electron beam deposition, atomic layer deposition, *etc.*, along with multi-step photolithographic mask patterning techniques. The entire process consumes both time and energy while having a low throughput. These factors thus increase the cost of manufacturing electronic devices. Printed electronics have garnered much attention since they offer a low cost alternative to conventional fabrication processes while enabling large-scale manufacturing of electronic devices. Compared to electrohydrodynamic jet (e-jet) printing and 3 dimensional printing, the large scale roll-to-roll printing of electronics takes advantage of the well-developed and low cost paper printing technologies to manufacture electronics and energy storage devices on various substrates.[1–7]

"Roll-to-roll" gravure printing is known for its high speed, fine dimensional capabilities, use of low viscosity inks, and vigorousness of the process. The typical gravure system comprises of an impression roll, an engraved gravure roll (image carrier), a doctor blade, and an ink pan. The surface of the gravure roll is engraved with the printing image and is responsible for transferring the ink from the ink pan to the substrate. The gravure roll is completely covered in ink and the excess ink on the roll is wiped off by the doctor blade. The impression roll is used to control the pressure and space between the substrate and the gravure roll. The substrate runs between the impression roll and the gravure roll. In this study, a laboratory scale gravure press was utilized to print a solution-based highly conductive silver nanoparticle ink that acts as the electrode for the radio frequency identification (RFID) antenna.

In order to implement roll-to-roll printing, the substrates are required to be stable and flexible, yet strong enough to be printable. Paper is a ubiquitous substrate for traditional printing due to its excellent printability and good flexibility. It is by far the cheapest biodegradable material that enables large-area printing for low cost disposable devices. However, for most multilayered printed electronics, the substrate needs to have minimum surface roughness or the device will result in a short circuit. In order to satisfy this requirement, plastic films are typically employed as the substrate for printed electronics. However, it is important to note that the large scale use of plastic causes build-up of non-biodegradable solid waste which poses significant threats to the natural environment. Additionally, the coefficient of thermal expansion (CTE) of plastic is considerably high, 20–100 ppm K^{-1}, which creates a substantial hurdle when working with high temperature fabrication processes.

Recently, robust transparent nanopaper with minimum surface roughness has attracted much attention as a suitable substrate for flexible electronics.[8–14] Nanopaper possesses tunable optical properties, high tensile strength, and a low surface roughness, all of which are favorable characteristics for

[a]*Department of Materials Science and Engineering, University of Maryland, College Park, Maryland 20742, USA. E-mail: binghu@umd.edu*

[b]*Department of Electrical and Computer Engineering, Western Michigan University, Kalamazoo, Michigan 49008, USA*

[c]*Department of Chemical and Paper Engineering, Western Michigan University, Kalamazoo, Michigan 49008, USA*

† Electronic supplementary information (ESI) available. See DOI: 10.1039/c4nr02036g

printing electronics.[15–17] Moreover, when compared to plastic, paper is biodegradable, sustainable, and recyclable. Transparent nanopaper also has several other advantages such as being low-cost, non-toxic, biocompatible for use in implantable biomedical electronic applications, and promising for visible packaging and biomedical sensing. However, one of the main obstacles for using nanopaper as a substrate in solution-based printing processes is the nanopaper's poor shape stability in solution. In this study, for the first time, the nanopaper was cross-linked to gain good shape stability for fully solution-based gravure printing. This work paves the way to develop transparent nanopaper which is capable of superseding plastic to create greener electronics.

Materials and experiment

Glutaraldehyde was purchased from Sigma Aldrich and used without further treatment. The water based silver ink HPS-030LV was supplied from Novacentrix Corp. The gravure printing is demonstrated with a Laboratory gravure press K-Printing Proofer (by Testing Machines Inc.)

2,2,6,6-Tetramethylpiperidinyloxy (TEMPO)-mediated oxidation was applied to the cellulose with NaClO and catalytic amounts of TEMPO and NaBr according to the previously reported methods.[10,11,16,18] Bleached Kraft softwood pulp extracted from the southern yellow pine was treated with the TEMPO/NaBr/NaClO oxidation system. 0.5 mmol TEMPO and 5 mol NaBr were separately added into 5 g cellulose with 1% concentration in deionized water, and the mixtures were stirred continuously for 10 min at 700 rpm with a Turrax mixer (IKA, RW20 digital) to form a uniform suspension. Thirty-five milliliters of sodium hypochlorite (NaClO) with a concentration of 12.5 wt% was titrated into the above mentioned suspension. The reaction time was monitored and the pH of the reaction system was kept constant at 10.5. The reaction lasted for approximately 3–4 h; however, the mixture was continuously stirred at 700 rpm for an additional 4 h to ensure adequate reaction of the wood fibers. The TEMPO-oxidized wood fiber solution was pumped once through a Microfluidizer processor (M110EH, Microfluidics Inc., USA) under a process pressure of 20 000 psi.

The obtained nanocellulose fiber was diluted to approximately 0.2 wt% in solution with deionized water, and 1% glutaraldehyde was added to the nanocellulose solution. The solution was filtered through the membrane (0.65 μm, PVDF) and 1 ml HCl solution was added during the filtration process. The whole crosslinking process took 1–2 h.

The nanopaper surface energy was tested by using a First Ten Angstrom (FTA 200) dynamic contact angle measuring device. The testing syringe was filled with the desired liquid. All the trapped air-bubbles in the syringe were removed by pumping out the liquid. The surface of the syringe was cleaned with a lint-free tissue Kimwipe. For water, a needle with an outer diameter range of 0.6 mm was used and for methylene iodide a diameter of approx 0.5 mm was used. The surface energies for both the substrates were calculated with the Owens–Wendt method.

Results and discussion

Good shape stability in solution is required for the substrate in high resolution electronic printing. In the printing process, the substrate is typically in contact with the ink solution. If the substrate does not have good shape stability, it will wrinkle resulting in a short circuit. Especially with the development of advanced nano-inks such as graphene ink or carbon nanotube (CNT) ink, the importance of a stable substrate is evident.[19–21] Even though the transparent nanopaper offers many beneficial properties, such as tunable optical properties and high mechanical strength, the nanopaper is not shape stable in water. Cellulose is hydrophilic due to the large amount of hydroxyl groups, which adsorb and hold water efficiently. Therefore, the shape of the nanopaper changes dramatically after immersing in water. In this work, glutaraldehyde was used as the crosslinking agent to block the exposure of hydroxyl groups to the solvent, and therefore improve the shape stability of nanopaper in water. The nanocellulose fiber was prepared with TEMPO/NaBr/NaClO oxidation system and microfluidizer (M110EH, Microfluidics Inc., USA) homogenization.[10,11,16,18] The obtained nanocellulose fiber was diluted to approximately 0.2 wt% in deionized water, and 0.5 wt% glutaraldehyde (Sigma Aldrich, US) was added to the nanocellulose solution. The solution was filtered through a membrane (0.65 μm, PVDF) and two drops of hydrochloric acid were added to yield a solution of pH $\sim$ 3. Crosslinking occurred when the cellulose was mixed with glutaraldehyde in an acidic environment.

Glutaraldehyde is widely used as an agent for polymer crosslinking.[22–24] Fig. 1(a) and (b) shows the nanopaper without and with crosslinking treatment before being immersed in water. The two nanopapers have a similar appearance with high transmittance and a 30 μm thickness. After immersing the nanopaper in water for 24 h, the nanopaper without the glutaraldehyde treatment, shown in Fig. 1(c), swelled to 6 mm, which was 200 times thicker than the original paper. However, it was observed that the dimensions of the nanopaper with the crosslinking treatment were stable in water. After the same 24 h immersion in water, the paper thickness experienced a small increase to 33 μm, as seen in Fig. 1(d). It is thus apparent that the glutaraldehyde treatment increased the nanopaper's shape stability in water dramatically.

With the decrease of the fiber diameter, more hydroxyl groups are exposed to the solvent, which causes a powerful interaction between the cellulose and the surrounding environment. During the glutaraldehyde treatment depicted in Fig. 1(e), the hydroxyl groups react with the aldehydes to create a cross-linked structure, blocking a majority of the hydroxyl groups, and therefore have a better shape stability in water. The paper without the crosslinking treatment is not stable in water due to the reaction between the hydroxyl groups and water. The cross-linked structure obtained creates enhanced shape stability for the nanopaper, which promotes the application of nanopaper for solution based printing of electronics.

From the FTIR spectra (Fig. 2(a)), typical vibration peak bands were observed for the cellulose, before and after

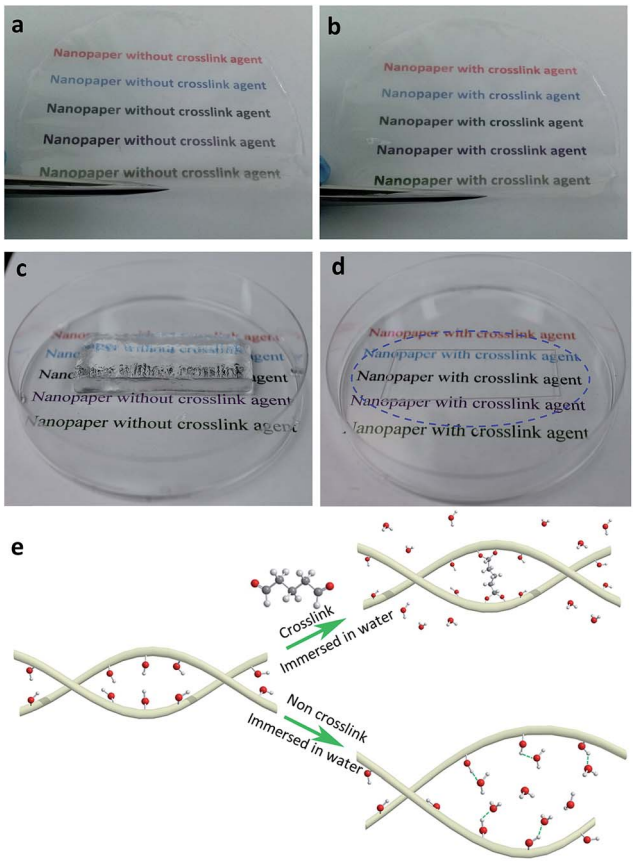

Fig. 1 (a) An image of transparent, flexible nanopaper without the crosslinking treatment. (b) An image of nanopaper after the crosslinking treatment. The nanopapers with and without crosslinking treatment have similar appearance before being immersed in water. (c) An image of nanopaper without the crosslinking treatment being immersed in water for 24 h. The thickness of the nanopaper expanded from ~30 μm to ~6 mm. (d) An image of nanopaper with the crosslinking treatment immersed in water for 24 h. (e) Schematic to show the mechanism of shape stability improvement after glutaraldehyde treatment.

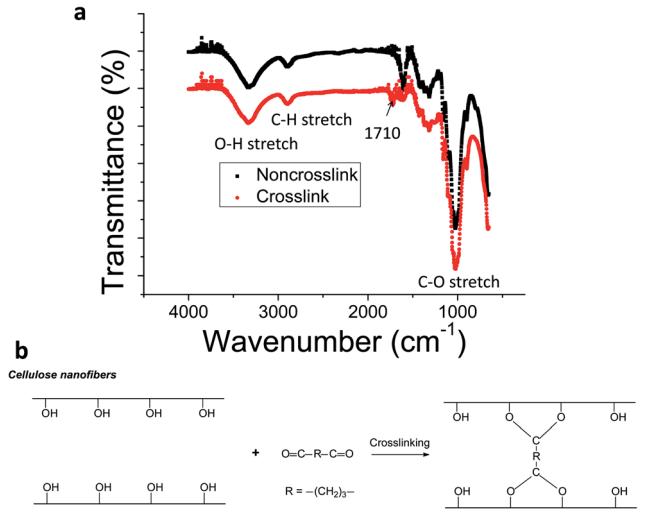

Fig. 2 (a) FTIR spectra of non-crosslinking and crosslinking nanopaper. (b) Crosslinking reaction between the cellulose and glutaraldehyde.

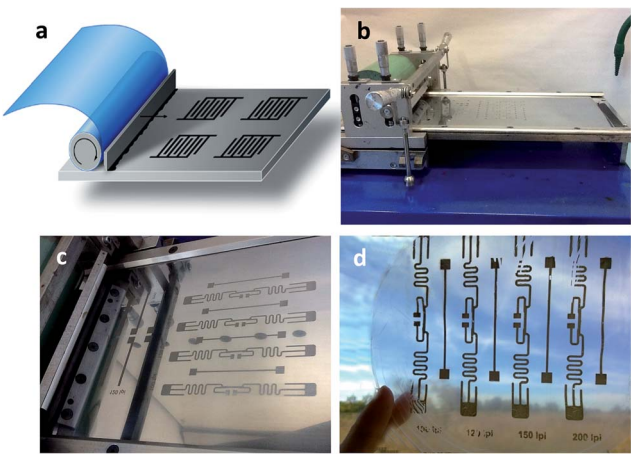

Fig. 3 (a) Schematic of the laboratory gravure press K-Printing Proofer. (b) An image of the laboratory gravure press K-Printing Proofer. (c) An image of the RFID antenna printing pattern on the engraved plate. (d) An image of 4 RFID antennas on transparent nanopaper. The printing video is elucidated in the ESI.†

crosslinking, in the range 2860–2900 cm^{-1} assigned to C–H, 3400 cm^{-1} assigned to O–H vibrations, and 1000–1100 cm^{-1} assigned to the C–O stretch.[25] Meanwhile, an increased absorption was also observed at 1710 cm^{-1}, which can be attributed to the acetate bridge.[22,26] The dialdehyde group from glutaraldehyde reacted with the hydroxyl group from cellulose to form an acetate bridge. The peak obtained at 1710 cm^{-1} indicates the cross-linking reaction. Mansur *et al.* determined the amount of acetate bridges with the absorption bands of 1710 cm^{-1} in preparing hydrogels based on glutaraldehyde-crosslinked poly(vinyl alcohol).[26] In the present study, the IR spectra indicated that the crosslinked nanopaper was prepared successfully. The mechanism of the crosslinking reaction was predicted as shown in Fig. 2(b).

Fig. 3(a) shows schematic of the laboratory gravure press K-Printing Proofer, which uses a plate instead of a cylinder engraved with the printing pattern to transfer the ink. The printing paper is fixed on the impression roll and the ink is applied on the image carrier panel. During printing, the impression roll, the paper, and the doctor blade move forward causing the pattern to transfer from the panel to the substrate with a fine resolution of 200 lines per inch and a maximum height of 40 μm. Simultaneously, the doctor blade wipes off the excess ink. The printing speed can reach 40 m min^{-1} and a printing video is available in the ESI.† Fig. 3(b) depicts the printing equipment in its entirety: the impression cylinder, the doctor blade, and the image carrier panel. Fig. 3(c) shows an engraved 4 RFID antenna pattern. The engraved plate can be switched to compensate for different patterns for various devices including sensors, transistors, capacitors, and batteries. Fig. 3(d) shows the printed antennas on the transparent nanopaper. The printed line has a sheet resistance of 0.3 ohms per sq. The antenna has the potential to be applied in advanced

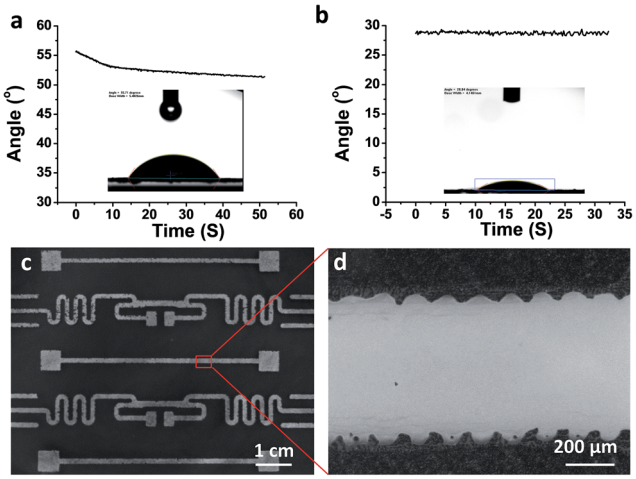

Fig. 4 Substrate surface energy and ink resolution characterization. (a) The dynamic contact angles for the water droplet; (b) the dynamic contact angles for the methylene iodide droplet; (c and d) microscopic observation of the printed lines on the nanopaper and a magnified image.

devices such as WiMAX applications, integrated solar modules, CubeSats, *etc.*[27–32] Additionally, the antenna printed on the flexible nanopaper enables devices to be foldable for applications in origami electronics.[13]

Surface energy is a key parameter used to characterize the printability of substrates. The surface tension of the liquid was calculated by the pendant drop method. The surface energy and surface tension measurements determine the amount of wetting and spreading, which influences the printing quality. Fig. 4(a) shows a distinct change in the water's contact angle against time which is indicative of substantial wetting of the substrate. As shown in the inset image, the mean contact angle of the water on the nanopaper is 52.9°. Comparatively, the methylene iodide contact angle shown in Fig. 4(b) is 28.8°, which is much lower when compared to that of water. The surface energy of the nanopaper, calculated with Owens–Wendt calculation, is 53.55 mN m^{-1}, which is much higher than polyethylene terephthalate (PET) (36–45 mN m^{-1}). Considering this surface energy, the nanopaper will be more compatible with water-based ink systems. If the surface energy is very high and there is a large amount of liquid penetration, there will be a larger amount of spreading of the ink on the substrate which may result in unfavorable print resolutions. Thus, the ink spread for a traditional paper-based substrate will be comparatively higher than our nanopaper due to more liquid penetration which may decrease the thickness of the ink film, thereby reducing the electrical performance of the ink. Fig. 4(c) shows the nanopaper with silver nanoparticle printed lines produced using gravure printing. Fig. 4(d) is a magnified image that shows the high resolution printing line with clear printing edges.

The Alien Technology UHF RFID tag "squiggle" (2nd generation) antenna design was used as the pattern for our printed antenna. An Agilent 4396B network analyzer was used to test the RF performance of the printed antenna. A fixed reference

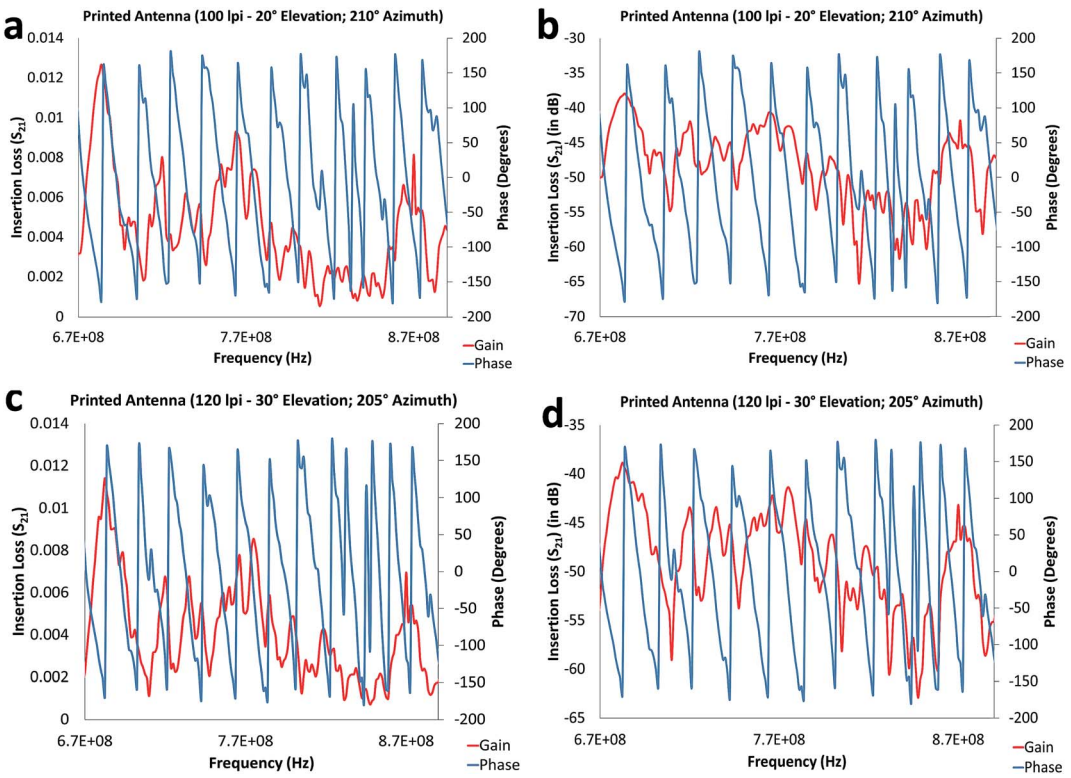

Fig. 5 RF response of the 100 lpi gravure printed antenna: (a) insertion loss and (b) insertion loss (S_{21}) in dB. RF response of the 120 lpi gravure printed antenna: (c) insertion loss (S_{21}) and (d) insertion loss (S_{21}) in dB.

antenna was placed at a defined distance of 3.6 m from the printed antenna. The printed antenna was mounted on top of a movable pedestal (DAMS 5000 Standard Measurement System from Diamond Engineering) capable of moving in the *X*–*Y* directions (*X*-azimuth: 0°–360°, *Y*-elevation: ±45°). The Antenna Measurement Studio 5.999X software (Diamond Engineering) was utilized to program the movement of the movable pedestal, as well as to acquire and analyze the RF response of the printed antenna. The performance of the printed antenna was tested in the RF range from 0.5 GHz to 1.5 GHz for azimuths and elevations ranging from 0° to 360° and −30° to +30°, respectively. It was observed that the maximum gain was obtained at +20° elevation; 210° azimuth (Fig. 5(a)) and +30° elevation; 205° azimuth (Fig. 5(c)) for the 100 lpi and 120 lpi, respectively at a resonant frequency of 683.75 MHz. These results demonstrate that the insertion losses for the 100 lpi and 120 lpi were −37.9 dB (Fig. 5(b)) and −38.85 dB (Fig. 5(d)), respectively for the maximum gains obtained at 683.75 MHz. The RF based response of the printed antenna demonstrates the feasibility of using large-scale printing technologies to fabricate flexible RFID antennas suitable for various electronic applications.

Compared to conventional electronic manufacturing processes, printing techniques not only reduce fabrication time but also the cost to fabricate electronic devices. Reliable RFIDs have wide applications in identification and sensing operations. Notably, the K-proofer gravure printing process used in this study has the potential for adaptation to large scale roll-to-roll printing setups enabling higher outputs and larger devices. Meanwhile, the printing process used for the stable nanopaper substrate can be applied towards fabricating multilayered devices with other well-developed printing methods such as screen printing and ink-jet printing. This work presents an important advancement towards the practical use of a transparent nanopaper substrate for printable and flexible electronics.

Conclusions

In summary, the shape stability of the transparent nanopaper in water was dramatically improved by using glutaraldehyde as a crosslinking agent to block most of the hydroxyl groups. Flexible antennas were fabricated by printing silver nanoparticle ink onto the stable, transparent nanopaper *via* gravure printing. The RF performance of the printed devices demonstrated their capability to be used as RFID antenna tags. The nanopaper's appropriate surface energy and good shape stability endow the device a good performance, especially with water-based ink. These results indicate the feasibility of using cross-linked nanopaper to fabricate devices by printing techniques such as gravure. As part of future work, further research is in progress in our lab to better understand the sensing mechanism and to investigate the effects of substrate bending on the performance of the printed antenna on the nanopaper substrate.

Acknowledgements

L. Hu acknowledges the support from the DOD (Air Force of Scientific Research) Young Investigator Program (FA95501310143). We acknowledge the Biotechnology Research and Education Center for letting us to use their Microfluidizer. We acknowledge Sai Guruva Avuthu Reddy, Jiaqi Dai, Xiaogang Han, Yuanyuan Li, and Bradley J. Bazuin for their contributions to this study. We also acknowledge the discussions with Dr Qian Yang (Department of Civil and Environmental Engineering, University of Maryland) regarding cross-linking.

References

1 J.-U. Park, S. Lee, S. Unarunotai, Y. Sun, S. Dunham, T. Song, P. M. Ferreira, A. G. Alleyene, U. Paik and J. A. Rogers, *Nano Lett.*, 2010, **10**, 584–591.
2 G. M. Neelgund, V. N. Bliznyuk, A. A. Pud, K. Y. Fatyeyeva, E. Hrehorova and M. Joyce, *Polymer*, 2010, **51**, 2000–2006.
3 B. B. Narakathu, S. G. A. Reddy, M. Z. Atashbar, E. Rebrosova, M. Rebros and M. K. Joyce, *A novel gravure printed impedance based flexible electrochemical sensor*, 2011.
4 P. H. Lau, K. Takei, C. Wang, Y. Ju, J. Kim, Z. Yu, T. Takahashi, G. Cho and A. Javey, *Nano Lett.*, 2013, **13**, 3864–3869.
5 Z. Li, R. Zhang, K.-S. Moon, Y. Liu, K. Hansen, T. Le and C. P. Wong, *Adv. Funct. Mater.*, 2013, **23**, 1459–1465.
6 B. Y. Ahn, E. B. Duoss, M. J. Motala, X. Guo, S.-I. Park, Y. Xiong, J. Yoon, R. G. Nuzzo, J. A. Rogers and J. A. Lewis, *Science*, 2009, **323**, 1590–1593.
7 K. Sun, T.-S. Wei, B. Y. Ahn, J. Y. Seo, S. J. Dillon and J. A. Lewis, *Adv. Mater.*, 2013, **25**, 4539–4543.
8 A. N. Nakagaito, M. Nogi and H. Yano, *MRS Bull.*, 2010, **35**, 214–218.
9 M.-C. Hsieh, C. Kim, M. Nogi and K. Suganuma, *Nanoscale*, 2013, 9289–9295.
10 H. Zhu, Z. Xiao, D. Liu, Y. Li, N. J. Weadock, J. Huang, L. Hu and Z. Fang, *Energy Environ. Sci.*, 2013, **6**(7), 2105–2111.
11 J. Huang, H. Zhu, Y. Chen, C. Preston, K. Rohrbach, J. Cumings and L. Hu, *ACS Nano*, 2013, **7**, 2106–2113.
12 H. Koga, M. Nogi and N. Komoda, *NPG Asia Materials*, 2014, **6**, 1–8.
13 M. Nogi, N. Komoda, K. Otsuka and K. Suganuma, *Nanoscale*, 2013, **5**, 4395–4399.
14 Y. H. Zhou, C. Fuentes-Hernandez, T. M. Khan, J. C. Liu, J. Hsu, J. W. Shim, A. Dindar, J. P. Youngblood, R. J. Moon and B. Kippelen, *Sci. Rep.*, 2013, **3**.
15 Z. Fang, H. Zhu, Y. Yuan, D. Ha, S. Zhu, C. Preston, Q. Chen, Y. Li, X. Han, S. Lee, G. Chen, T. Li, J. Munday, J. Huang and L. Hu, *Nano Lett.*, 2013, 765–773.
16 H. Zhu, S. Parvinian, C. Preston, O. Vaaland, Z. Ruan and L. Hu, *Nanoscale*, 2013, **5**, 3787–3792.
17 M. Henriksson, L. A. Berglund, P. Isaksson, T. Lindstrom and T. Nishino, *Biomacromolecules*, 2008, **9**, 1579–1585.
18 Z. Fang, H. Zhu, C. Preston, X. Han, Y. Li, S. Lee, X. Chai, G. Chen and L. Hu, *J. Mater. Chem. C*, 2013, **1**, 6191–6197.
19 E. B. Secor, P. L. Prabhumirashi, K. Puntambekar, M. L. Geier and M. C. Hersam, *J. Phys. Chem. Lett.*, 2013, **4**, 1347–1351.
20 X. Han, Y. Chen, H. Zhu, C. Preston, J. Wan, Z. Fang and L. Hu, *Nanotechnology*, 2013, **24**, 205304.

21 L. Hu, J. W. Choi, Y. Yang, S. Jeong, F. La Mantia, L.-F. Cui and Y. Cui, *Proc. Natl. Acad. Sci. U. S. A.*, 2009, **106**, 21490–21494.
22 S. Rimdusit, K. Somsaeng, P. Kewsuwan, C. Jubsilp and S. Tiptipakorn, *Eng. J.*, 2012, **16**, 15–28.
23 S. Distantina and M. Fahrurrozi, *Int. Proc. Chem., Biol. Environ. Eng.*, 2012, **38**, 150.
24 C. K. Chan, H. L. Peng, G. Liu, K. McIlwrath, X. F. Zhang, R. A. Huggins and Y. Cui, *Nat. Nanotechnol.*, 2008, **3**, 31–35.
25 L. Tomé, L. Brandão, A. Mendes, A. D. Silvestre, C. Neto, A. Gandini, C. R. Freire and I. Marrucho, *Cellulose*, 2010, **17**, 1203–1211.
26 H. S. Mansur, C. M. Sadahira, A. N. Souza and A. A. P. Mansur, *Mater. Sci. Eng. C*, 2008, **28**, 539–548.
27 A. S. Azini, M. R. Kamarudin, T. A. Rahman, H. U. Iddi, A. Y. Abdulrahman and M. F. Jamlos, *Prog. Electromagn. Res.*, 2013, **138**, 133–141.
28 B. M. Levin, *J. Commun. Technol. Electron.*, 2012, **57**, 388–392.
29 N. Guan, H. Furuya, K. Himeno, K. Goto and K. Ito, *IEICE Trans. Comm.*, 2007, **E90B**, 2219–2224.
30 C. C. Serra, C. R. Medeiros, J. R. Costa and C. A. Fernandes, *IEEE Antenn. Wireless Propag. Lett.*, 2011, **10**, 776–779.
31 A. Katsounaros, Y. Hao, N. Collings and W. A. Crossland, *Electron. Lett.*, 2009, **45**, 722–723.
32 E. H. Lim and K. W. Leung, *IEEE Trans. Antennas Propag.*, 2010, **58**, 1054–1059.